# A new method for the retrieval of the equivalent refractive index of atmospheric aerosols

S. Vratolis[☆1,2], P. Fetfatzis[1], A. Argyrouli[2], A. Papayannis[2], D. Müller[5], I. Veselovskii[10,11], A. Bougiatioti[2,3,4], A. Nenes[4,6,7,8], E. Remoundaki[9], E. Diapouli[1], M. Manousakas[1], M. Mylonaki[2], K. Eleftheriadis[1]

[1]*ERL, Institute of Nuclear & Radiological Sciences & Technology, Energy & Safety, National Centre of Scientific Research Demokritos, 15310 Ag. Paraskevi, Attiki, Greece*
[2]*Laser Remote Sensing Unit, Physics Department, School of Applied Mathematics and Physical Sciences, National Technical University of Athens (NTUA), 15780 Zografou, Greece*
[3]*ECPL, Department of Chemistry, University of Crete, Voutes, 71003 Heraklion, Greece*
[4]*School of Earth & Atmospheric Sciences, Georgia Institute of Technology, Atlanta, GA 30332, USA.*
[5]*School of Physics, Astronomy and Mathematics, University of Hertfordshire, Herts AL 10 9AB, UK*
[6]*ICE-HT, Foundation for Research and Technology, Hellas, 26504 Patras, Greece*
[7]*Institute of Environmental Research and Sustainable Development, National Observatory of Athens, Athens, Greece*
[8]*School of Chemical & Biomolecular Engineering, Georgia Institute of Technology, Atlanta 30332, GA, USA*
[9]*Laboratory of Environmental Science and Engineering, School of Mining and Metallurgical Engineering, National Technical University of Athens, 15780 Zografou, Greece*
[10]*Physics Instrumentation Center of GPI, Troitsk, Moscow, Russia*
[11]*Joint Center for Earth Systems Technology, UMBC, Baltimore, USA*

**Abstract**

In the context of the international experimental campaign Hygroscopic Aerosols to Cloud Droplets (HygrA-CD, 15 May to 22 June 2014), dry aerosol size distributions were measured at Demokritos station (DEM) using a Scanning Mobility Particle Sizer (SMPS) in the size range from 10 to 550 nm (electrical mobility diameter), and an Optical Particle Counter (OPC model Grimm 107 operating at the laser wavelength of 660 nm) to acquire the particle size distribution in the size range of 250 nm to 2.5 $\mu$m optical diameter. This work describes a method that was developed to align size distributions in the overlapping range of the SMPS and the OPC, thus allowing for the retrieval of an aerosol equivalent refractive index (ERI). The objective is to show that size distribution data acquired at in situ measurement stations can provide an insight to the physical and chemical properties of aerosol particles, leading to better understanding of aerosol impact on human health and earth radiative balance. The resulting ERI could be used in radiative transfer models to assess aerosol forcing direct effect, as well as an index of aerosol chemical composition. To validate the method, a series of calibration experiments were performed using compounds with known refractive index (RI). This led to a corrected version of the ERI values, ($ERI_{COR}$). The $ERI_{COR}$ values were subsequently compared to model estimates of RI values, based on measured $PM_{2.5}$ chemical composition, and to aerosol RI retrieved values by inverted lidar measurements on selected days.

*Keywords:*
Aerosol refractive index
Urban background aerosol
Scanning Mobility Particle Sizer
Optical Particle Counter
Lidar
Aerosol size distribution

## 1. Introduction

The refractive index of a medium is a pure number that describes how fast light propagates through it. The light intensity scattered by an aerosol particle in all angles can be calculated by the Mie theory, provided the particle is spherical, and that its refractive index and geometric diameter are known (Bohren and Huffman, 1998).

Instruments used for the measurement of the aerosol size distribution have different measurement techniques, each depending on another aerosol property. The Scanning Mobility Particle Sizer (SMPS) measures the number concentration in a range of electrical mobility diameters. An Optical Particle Counter (OPC) measures the optical size of aerosols, which depends on the particle refractive index, geometric size and shape. These quantities are generally unknown for atmospheric particles. Constructing a complete size distribution from 10 nm up to 1 $\mu$m requires that distributions are in agreement in the overlapping range. The threshold of 1 $\mu$m was used due to increasing uncertainty of OPC measurements above this geometric diameter (Heim et al., 2008). Here we propose a new method to reconcile overlapping data, yielding size distribution up to 1 $\mu$m with respect to geometric diameter. The method also yields an equivalent refractive index (ERI) corresponding to the common fraction of the size distributions measured by the two instruments. The derived ERI can be used to perform radiative calculations and understand the direct effect of aerosols in climate forcing. Several methods for retrieving refractive index are currently available. In one method, (Hand and Kreidenweis, 2002) have used OPC, SMPS, and Aerodynamic Particle sizer (APS) data to retrieve simultaneously the real part of refractive index and the effective density of aerosols. In another method, (Stelson, 1990) calculated the refractive index, based on the chemical composition. However, the optical properties of aerosols can highly depend on the degree of particle's mixing and the physical position of absorbing specie's aggregates with respect to host particles (Fuller et al., 1999). Refractive indices derived from chemical measurements can be used to invert OPC data; moreover, chemical data during the campaign existed as integrated 3 hour (3hr), 5hr, and 24hr samples and the variability in OPC distribution is often observed in finer time resolutions.

☆Corresponding Author
Email address: vratolis@ipta.demokritos.gr (S. Vratolis)

## 2. Experimental Procedure

The international experimental campaign Hygroscopic Aerosols to Cloud Droplets (HygrA-CD), organized in the Athens Metropolitan Area (AMA), Greece, from 15 May to 22 June 2014, provided an extended record of data on aerosols and their role in cloud formation (Papayannis et al., 2017). The major sampling site of the campaign was the Demokritos station (DEM), member of the GAW and ACTRIS Networks (37.995° N 23.816° E, at 270 m a.s.l), which is situated on the foot of Mount Hymettus in Agia Paraskevi. The DEM monitoring site belongs to the National Centre of Scientific Research Demokritos, which is situated about 7 km to the north from downtown Athens, in a pine forest. It is representative of the atmospheric aerosol at suburban areas of the Athens Metropolitan area. The station is frequently influenced by katabatic winds (Flocas et al., 1998), during which, air masses from mount Hymettus (peak height 1,024 meters) are brought over the station. Also, the lowering of nocturnal boundary layer height (NBLH) is occasionally resulting in an increase in particle number concentration, even in the absence of aerosol particle sources.

The instruments that were in operation during the campaign included:

1. an SMPS to acquire the particle size distribution of atmospheric aerosol in the size range from 10 to 550 nm (electrical mobility diameter). The instrument provides a full size distribution in the above mentioned range every 5 minutes. The SMPS has been calibrated against a reference SMPS system at the WCCAP (World Calibration Centre for Aerosol Physics) in 2013 and participated in an intercomparison workshop in 2016 at the WCCAP, exhibiting a counting accuracy within 10% for the size range 30-550 nm against a reference system under controlled laboratory conditions (Wiedensohler et al., 2012). The instrument is calibrated at DEM station

with PSL spheres that have an electrical mobility diameter of 200 nm.

2. an OPC (Grimm 107@660 nm laser light wavelength) to acquire the particle size distribution in the size range of 250 nm to 2.5 $\mu$m optical diameter. The OPC in a similar intercomparison at the WCCAP exhibited a counting accuracy within 10% for the size range 250 nm to 1 $\mu$m. This instrument acquires a full size distribution every 1 minute. The instrument uses laser light of 660 nm, opening angles detected are 29.5 ° - 150.5 ° and 81 ° - 99 ° (Bukowiecki et al., 2011). After its manufacture, the instrument follows an electronical adjustment of 1 $\mu$m channel with mono-disperse PSL 1 $\mu$m spheres (Duke Scientific, NIST traceable, m = 1.59, according to ISO 21501-1) (Schneider, 2016; Grimm Aerosoltechnik, 2005). Afterwards the unit is calibrated to a reference Grimm OPC, using dolomite aerosols (i.e. different refractive index and a full size distribution). The particle number concentration in each size bin of the unit is adjusted to the one measured by the reference instrument. The adjustment is performed by changing the detection limits thresholds for each size bin (Lymperopoulos, 2015; Schneider, 2016; Grimm-Aerosoltechnik, 2005). The reference Grimm OPC is checked and certified with monodisperse Latex aerosol (Grimm Aerosoltechnik, 2005). According to (Heim et al., 2008), the OPC counting accuracy is within 10% of the ideal 100% for sizes from 0.3 to 1 $\mu$m (electrical mobility diameter). The sizing accuracy decreases from around 0.8 $\mu$m up to approximately 2 $\mu$m.
3. an AE33 dual spot aethalometer in order to acquire the equivalent black carbon concentration (EBC) at seven wavelengths (370, 470, 520, 590, 660, 880, 950 nm). This instrument completes an EBC measurement for all wavelengths every 1 minute and operated after a $PM_{2.5}$ inlet.
4. an Ecotech 3-wavelength nephelometer to acquire the aerosol scattering and backscattering coefficient at 450, 525 and 625 nm. The instrument operated after a $PM_{10}$ inlet and completes a measurement for all wavelengths every 1 minute.
5. a Sunset Lab Elemental Carbon - Organic Carbon (EC/OC) measurement instrument. The instrument acquires one measurement every 3 hours. It operates after a $PM_{2.5}$ cyclone and it has participated in an intercomparison exercise (Panteliadis et al., 2015). During that exercise, the reproducibility relative standard deviation for all participants, was within 30%, without any correction applied.
6. a Droplet Measurement Technologies (DMT) streamwise thermal-gradient CCN counter. Throughout the campaign, the instrument was operated at a total flow rate of 0.5 LPM, with a sheath-to-aerosol flow ratio of 10:1, and a top-bottom column difference, $\Delta$ between 4 and 15 K. Concentrations were measured at each supersaturation for 10 min, yielding a CCN spectrum consisting of 5 different supersaturations every 50 min (Bougiatioti et al., 2017).
7. a multi-wavelength Raman lidar system (EOLE) deployed at the National Technical University of Athens (NTUA) (37.97° N, 23.79° E, 212 m a.s.l.), approximately 4 km from DEM station and 4.5 km from the city center which was used to provide the vertical profile of the optical properties of aerosols (backscatter and extinction coefficients) at 355-532-1064 nm (Kokkalis et al., 2012). Using these data as input, we can derive the vertical profile of the aerosol microphysical properties (i.e. refractive index, effective radius, volume concentration, etc.) based on inversion techniques (Mamun and Müller, 2016; Veselovskii et al., 2002).

Inlet aerosol flows are dried to relative humidity (RH) below 40%, while particle losses due to diffusion in the pipe lines are calculated and corrected for SMPS. Other losses are not corrected for the OPC and the SMPS, as their inlet line is vertical and therefore losses in the size range 0.2 to 1 $\mu$m (aerodynamic diameter) are not significant.

The analysis of $PM_{2.5}$ filters was performed by:

1. An accredited according to EN14902 high-resolution energy dispersive X-Ray fluorescence spectrometer Epsilon 5 by PANanalytical (XRF). Epsilon 5 is constructed with optimized Cartesian-geometrical design for lower

background and with extended K line excitation 100 kV X-ray capability. The spectrometer provides selection of 8 secondary targets ($Al$, $CaF_2$, $Fe$, $Ge$, $Zr$, $Mo$, $Al_2O_3$, $LaB_6$), that can polarize the X ray beam. All measurements were performed under vacuum (Emmanouil et al., 2017).

2. Ion Chromatography (IC). The concentrations of $Cl^-$, $NO_3^-$, $SO_4^{2-}$, $Na^+$, $K^+$, $NH_4^+$, $Ca^{2+}$, $Mg^{2+}$ were determined by a Metrohm 732 IC Separation Center connected to a 732 IC conductivity detector and a 753 Suppressor Module for anions determination as described in (Mantas et al., 2014).

## 3. ERI optimal solution algorithm

The aerosol particle's scattering process is described by four amplitude functions, $S_1$, $S_2$, $S_3$, $S_4$, all functions of $\theta$ (angle of incident light to scattered light in the direction of light propagation). Spherical particles have $S_3 = S_4 = 0$. So two complex amplitude functions occur for any direction; these functions are $S_1(\theta)$ and $S_2(\theta)$; they depend only on the scattering angle $\theta$. We have to compute the numbers (Hulst van de, 1981):

$$i_1 = |S_1(\theta)|^2 \; and \; i_2 = |S_2(\theta)|^2 \tag{1}$$

$$Q_{sca} = \frac{1}{x^2} \int_0^{\pi} \{i_1(\theta) + i_2(\theta)\} \sin(\theta) \, \mathrm{d}\theta \tag{2}$$

where x is the size parameter ($x = k_w r$, $k_w$ is the wave number and $r$ is the radius). $Q_{sca}$ is the scattering efficiency. Then we obtain the scattering effective cross section $S_{sca}$ by multiplying $Q_{sca}$ to the particle cross section area. The angular integration is performed over the solid angle corresponding to Grimm 107 (described earlier). The resulting scattering effective cross section $S_{sca}$, ($\mu m/m^2$), is calculated for each OPC size bin using the function Mie_*abcd* of (Mätzler, 2002).

The following assumptions apply for OPC measurements:

1. Absorption is negligible and particles are spherical.
2. The aerosol is internally mixed.
3. The size distribution measured by the OPC represents particles of sizes equivalent to those corresponding to PSL spheres with a real part of refractive index equal to 1.585 at 660 nm wavelength.

The fitting procedure consists of several steps. In the first step, the algorithm assumes that RI can range from 1.3 to 2.2 in steps of 0.1 (i.e. 1.3, 1.4, etc.). For these refractive indices, the Grimm size distribution is recalculated for size bins corresponding to SMPS. The Root Mean Square Error (RMSE) of the difference between the SMSP and OPC number size distributions (NSD) is calculated:

$$\mathrm{RMSE} = \frac{100}{\sqrt{\mathrm{n}}} \left( \sum_{i=1}^{n} \left[ N_{Di}^{SMPS} - N_{Di}^{OPC} \right]^2 \right)^{0.5} \tag{3}$$

where n is the number of size bins in the overlapping range of SMPS and OPC size distributions. $N_{Di}^{SMPS}$ is the number concentration measured by SMPS at size bin $i$ corresponding to particle diameter D and $N_{Di}^{OPC}$ is the number concentration measured by OPC at diameter D. The overlapping range varies with respect to the RI assumed. For assumed RIs below 1.3, the overlapping range has very few size bins. Subsequently, an algorithm is employed in order to find the ERI that minimizes RMSE (Nelder and Mead, 1965).

### *3.1. OPC diameter recalculation for assumed RIs*

Based on the assumptions mentioned earlier for the OPC, $S_{sca}$ is calculated for OPC size bins. $S_{sca}$ is not monotonically increasing with particle size, therefore it is fitted to the function

$$S_{sca} = a \, D^b \tag{4}$$

where D is particle diameter, and a,b derived fitted constants. This provides a good approximation in the particle size range from 100 - 1200 nm (Figures S5-S10). This approximation is from now on considered as the instrument primary measurement for each OPC size bin.

In order to invert the OPC size bins particle size for any other RI, we calculate $S_{sca}$ for a range of diameters extending from 100 to 1200 nm. Then, we

calculate the constants a,b in the $S_{sca}$ relation to diameter D for the new RI, according to equation 4. Subsequently, we find the particle size diameters corresponding to the OPC primary measured $S_{sca}$.

## 4. Method Evaluation - Calibration Procedure

In order to evaluate the method for the ERI retrieval, a series of calibration experiments were made. For this purpose, we generated test aerosol of known chemical composition.

Bulk materials were chosen from common chemical species found in the atmospheric aerosol or used in instrument calibration, with RI values according to the literature: Ammonium Sulfate (RI = 1.53@580 nm wavelength) (Tang, 1996), Di-Ethyl-Hexyl-Sebacate (RI = 1.45@650 nm) (TOPAS, 2008) and Polystyrene Latex Spheres (PSL) with sizes of 262 and 490 nm (RI = 1.585@660 nm) (Sultanova et al., 2009). Calculations of the response function were performed and ERI was calculated for each chemical compound.

Based on the PSL experiment it was concluded that $S_{sca}$ has to be corrected for a sizing error in OPC NSD, within the ERI retrieval algorithm according to equation 5.

$$S_{sca-cor} = \frac{S_{sca}}{1.5} \qquad (5)$$

The next step is to find a correction factor for aerosols with RI different from PSL spheres, incorporating all experiments. The final ERI correction equation for the dependence on aerosol RI follows:

$$RI = 1.7 \exp((-(ERI_{COR} - 2)/1.5)^2) \qquad (6)$$

The calibration procedure, setup, and results in detail are presented as supplementary material. Regression analysis of the literature RI and ERI derived from the calibration procedure, yielded an overall standard error of ± 0.1. The discrepancies between literature and calculated RI can be attributed to the OPC measurement principal and subsequent signal treatment by the instrument, which leads to a distortion of the particle size distribution for substances with RIs lower than 1.6.

The DEM station is a background station and the overlapping range of SMPS and OPC is in accumulation mode, therefore $ERI_{COR}$ is expected to frequently correspond to aged, internally mixed aerosol. Nevertheless, occasionally, particles might have variable RIs, even if they are measured in the same optical size range (externally mixed). The measurement error is expected to be higher in this situation.

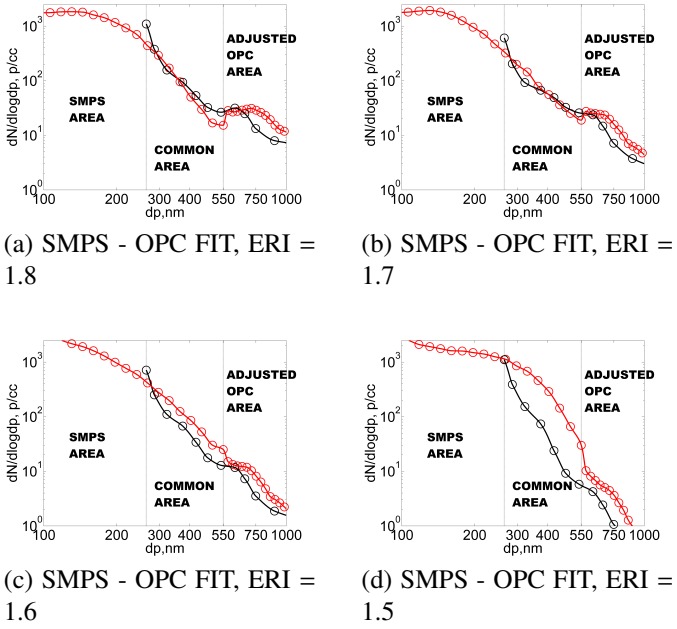


(a) SMPS - OPC FIT, ERI = 1.8

(b) SMPS - OPC FIT, ERI = 1.7

(c) SMPS - OPC FIT, ERI = 1.6

(d) SMPS - OPC FIT, ERI = 1.5

Figure 1: SMPS - OPC fit examples for various ERI values. Red circles and line denote the measured SMPS size distribution (SD) combined with the fitted Grim 107 size distribution, while the black circles and line represents the Grim 107 measured SD. The Grim 107 SD is moved to the right at ERI = 1.6, as it should, in order to compensate for the sizing error in relation to the SMPS observed at the PSL calibration experiment.

## 5. Major findings

After fitting the SMPS and the OPC size distributions obtained at DEM station during HygrA-CD campaign, we acquire the optimal solution ERI, as depicted in Figure 1. The correction of equation 6 has not yet been applied.

We observe that the original SMPS - OPC size distributions are quite different in these 4 cases, leading to large differences in ERI retrieved. In general, higher initial OPC NSD in the overlapping range corresponds to higher refractive index. That is because particles with high refractive index are classified as larger than they actually are by OPC. As we can also observe in Figure S11, adjustment of the two size distributions is very good, but the ERI retrieved

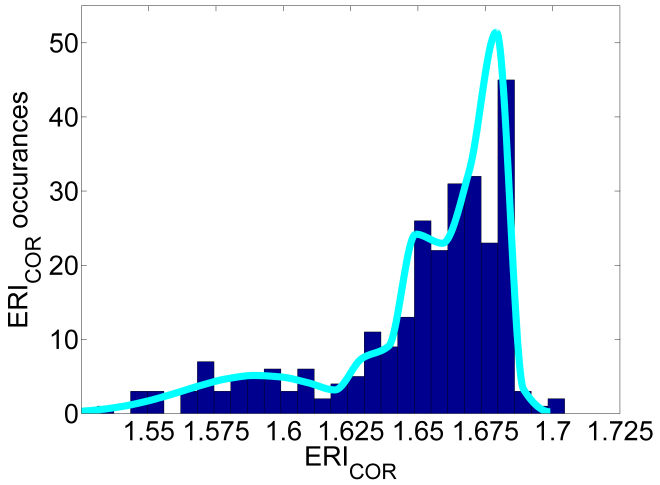


Figure 2: $ERI_{COR}$ histogram evolution of the 3h mean values during the whole period of HygrA-CD campaign. Blue boxes denote the number of $ERI_{COR}$ occurrences in each size bin, while the cyan line denotes the best fit of the histogram using Gaussian distributions.

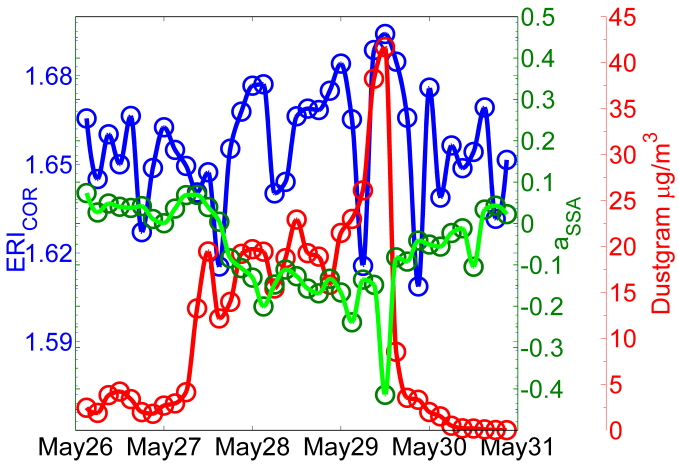


Figure 3: $ERI_{COR}$ (blue) in comparison to Single Scattering Albedo exponent ($a_{SSA}$, green) derived from DEM station instrument measurements. The SKIRON Sahara dust model output ($\mu g/m^3$) at 400 m above ground level (agl) is also depicted (red). Circles are actual data points, while lines are interpolation.Data are taken from 26 to 31 May 2014.

varies over a range of values wider than those reported in literature.

We have to keep in mind that the ERI is not the actual RI of the aerosol measured by SMPS and OPC, but rather a number describing the optimal solution of a fitting procedure between the size distributions of the two instruments. Particulate RI could be variable even within each size bin measured by the OPC. We expect it to be closely related to an average overall RI of the size distribution, but the relation might depend on factors like aerosol mixing state and the presence of more than one modes in the overlapping range. The transfer functions of the two instruments and subsequent data treatment, also lead to discrepancies in the size distributions measured. This optimal solution in Figure 1 includes the correction for the sizing error of the OPC.

In order to correct for the relation of ERI to RI, as observed in the calibration experiments, we apply equation 6 and acquire $ERI_{COR}$. An overview of $ERI_{COR}$ during HygrA-CD campaign is presented in Figure 2. The histogram of the measured values indicates that most of the values are in the range between 1.625 and 1.675.

### 5.1. $ERI_{COR}$ comparison to aerosol mass constituents

According to (Amato et al., 2016), dust constituted 12% of $PM_{2.5}$ mass during 2013 at the DEM station. In order to investigate if the presence of dust is indicated by $ERI_{COR}$, we calculated the Single Scattering Albedo Exponent $a_{SSA}$ at 450-625 nm wavelength. We accomplished that using data from the AE33 and the Ecotech Nephelometer.

In Figure 3 we observe that a Sahara dust episode is indicated on the 27th to 30th of May 2014 by SKIRON model (Kallos et al., 2006). When coarse particles are present (during Sahara dust events), $a_{SSA}$ becomes clearly negative with values usually falling between -0.1 and -0.5, according to (Coen et al., 2004). We observe in Figure 3 that when $a_{SSA}$ is below -0.1, $ERI_{COR}$ increases. This could be attributed to dust constituents with high RI. We should keep in mind that $ERI_{COR}$ and $a_{SSA}$ are derived from station measurements, which means that they represent the aerosol properties at the station level, while the model output represents an estimation of Sahara dust content at air masses above the station. We expect the $ERI_{COR}$ and the $a_{SSA}$ to be closely related, but this is sometimes not the case for the SKIRON model.

In order to compare the $ERI_{COR}$ to the aerosol

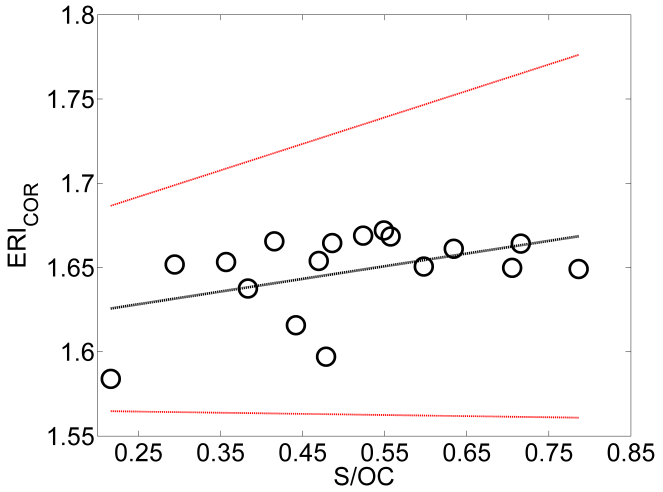


Figure 4: $ERI_{COR}$ 24hr averages in comparison to Sulfur per Organic Carbon mass ratio of aerosols up to 2.5 $\mu$m (aerodynamic diameter) during HygrA-CD campaign. Red lines depict the 95% confidence intervals.

composition, 24hr averages of $ERI_{COR}$ were obtained at the time intervals corresponding to XRF measurements. In Figure 4, the OC values were adjusted for carbon and hydrogen weights by multiplying with a mass correction factor of 1.4 (Hand and Kreidenweis, 2002).

When the Sulfur to Organic Carbon ratio increases, $ERI_{COR}$ increases, as sulfuric compounds have almost the same RI compared to organic compounds, but most organic compounds emission sources are associated with Elemental Carbon, the major absorbing species.

In order to compare $ERI_{COR}$ to aerosol composition, mineral dust (or soil dust) was estimated based on XRF measurements and average crust composition (Nava et al., 2012), as

$$\text{Mineral Dust} = 1.35\,Na + 1.66\,Mg + 1.89Al + 2.14\,Si + 1.21\,K + 1.40\,Ca + 1.67\,Ti + 1.43\,Fe \quad (7)$$

Some corrections were however applied to this formula to take into account sea-salt contributions to $Na$ and $Mg$, and possible anthropogenic contributions to the other elements. The sea salt fractions of $Na$ and $Mg$ were calculated using the measured $Cl$ concentration and the $Na/Cl$ and $Mg/Cl$ ratios 0.56 and 0.07, respectively. Due to possible $Cl$ losses in aerosol samples, this approach may overestimate the non-sea salt component of $Na$ ($nss_{Na}$) and $Mg$ ($nss_{Mg}$).

Table 1: Physical constants of species used in refractive index and density calculations (Hand and Kreidenweis, 2002) and (Kandler et al., 2007).

| Species | Density (g $cm^{-3}$) | Refractive index |
|---|---|---|
| $(NH_4)_2\,SO_4$ | 1.76 | 1.53 |
| $NaNO_3$ | 2.26 | 1.59 |
| Organic Carbon | 1.40 | 1.55 |
| Elemental Carbon | 2.00 | 1.96 – 0.66 i |
| Mineral dust | 1.99 | $1.59 - 7 * 10^{-3}$ |

### 5.2. $RI_{IC}$ acquired by Ion Chromatography, EC/OC and dust measurements

A filter sampler was deployed at the National Technical University of Athens (NTUA) (37.97° N, 23.79° E, 212 m a.s.l.), approximately 4 km from DEM station. Ion Chromatography was used in order to separate anions and kations of the aerosol collected. The model ISORROPIA (II) (Fountoukis and Nenes, 2007) was applied to the results and the water content of the aerosol species was calculated. The RH and temperature used were the average of the ones recorded at DEM station SMPS and OPC inlet line, at the corresponding time intervals. Based on the assumption that during daytime, the air masses over the GAA are well mixed, we also used the EC/OC measured at DEM station. Dust derived at the DEM station was also used, but we have to keep in mind that it is derived from filter samples with 24hr duration. Two samples were excluded, as at the time of measurement there was strong mixing in the vertical, bringing aerosol from higher layers (probably dust), leading to very high $ERI_{COR}$ values, not corresponding to 24hr averages of dust concentration (Figures S12, S13).

The density and refractive index data for the mass constituents calculated are presented in Table 1.

According to (Kandler et al., 2007), the imaginary part strongly decreases with increasing particle size, reflecting the fact that the highly absorbing components (hematite and soot) are predomi-

nantly found in the small particle range. Therefore, at the size range that $ERI_{COR}$ is calculated (approximately 260-550 nm electrical mobility diameter), we expect significant absorption. This is attributed not only to the dust absorption, but also to the fact that during Sahara dust events the Planetary Boundary Layer Height (PBLH) reduces significantly according to (Banks et al., 2016), leading to higher concentrations of pollutants, including EC. Despite all that, the $ERI_{COR}$ values increase during dust events (see Figure 3), as it appears that the effect of constituents with high real part of RI like dolomite (RI = 1.62), calcite (RI = 1.6), chloritoid (RI = 1.73), hematite (3.05 - 0.3 i) and ilmenite (2.4 - 0.3 i) is significant (Kandler et al., 2007).

The aerosol density was computed from the chemical analysis data following (Hasan and Dzubay, 1983) using Equation 8:

$$\rho^{-1} = \sum_i \frac{X_i}{\rho_i} \tag{8}$$

where $X_i$ is the mass fraction for species i and $\rho_i$ is the individual species density ($gcm^{-3}$). Refractive index can be computed by different mixing rules, 2 of which are partial molar refraction (Stelson, 1990) and volume-weighted method (Hasan and Dzubay, 1983).

The volume-weighted method was used (Equation 9) to calculate mean refractive index ($m = m_r - k_i$).

$$m = \rho \sum_i \frac{X_i m_{r,i}}{\rho_i} - \rho \sum_i \frac{X_i k_i}{\rho_i} i \tag{9}$$

where $m_r$ is the real part of a complex refractive index for species i and $k_i$ is the imaginary part. The only absorbing species included were EC and Dust. The imaginary part of the refractive index was not calculated, as it could not be compared to $ERI_{COR}$.

In Figure 5, $ERI_{COR}$ and $RI_{IC}$ seem to have a standard offset during these hours (around 0.05-0.1). $ERI_{COR}$ and $RI_{IC}$ are well correlated ($R^2$ = 0.88 for a linear fit). We also observe that when there is large EC content, $ERI_{COR}$ is lower, regardless of the dust mass in the particles.

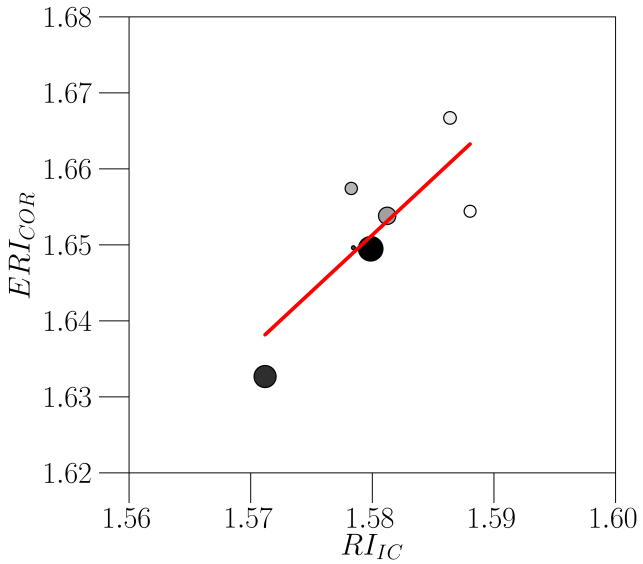


Figure 5: $ERI_{COR}$ averages in comparison to $RI_{IC}$ derived from IC, EC/OC and XRF measurements during HygrA-CD campaign. The red line depicts the linear fit for the data points. The size of the markers corresponds to dust content (larger means more dust mass), while the color corresponds to EC content (darker means more EC mass).

### *5.3. Lidar inversion algorithm description to acquire aerosol $RI_{LI}$ and comparison to $ERI_{COR}$*

The 6-wavelength Raman lidar system (EOLE) was operated at National Technical University of Athens (NTUA) (37.97° N, 23.79° E, 212 m a.s.l.), during selected daytime/nighttime slots (37 days and nights out of 39), to provide the vertical profiles of the aerosol backscatter coefficient ($b_{aer}$) (at 355, 532 and 1064 nm) and aerosol extinction coefficient ($a_{aer}$) (at 355 and 532 nm), the lidar ratio (S = $a_{aer}/b_{aer}$) (at 355 and 532 nm), and the aerosol Ångström exponent $AE$-related to backscatter and extinction coefficients. During nighttime the vertical profiles of $b_{aer}$, $a_{aer}$, $S$, and $AE$-related to extinction and backscatter coefficients are retrieved with 10-20%, 10-15%, 10% and 25% uncertainty, respectively (Kokkalis et al., 2012).

During daytime, using as input a constant $S$ value (constrained by the mean Aerosol Optical Depth ($AOD$) value obtained from a nearby sunphotometer), we retrieve only the $b_{aer}$ and the $AE$-related to backscatter coefficient values with an average uncertainty (due to both statistical and systematic errors) of 20-30% and 25%, respectively (Kokkalis et al.,

2012). Moreover, EOLE provided the water vapor mixing ratio profiles from 0.5 to 6-7 km height, during nighttime, with a statistical error less than 8% at heights up to 2 km and 10-15% from 2.5 to 6 km (Mamouri et al., 2007).

Although full overlap of EOLE occurs at 600-700 m above ground level, an experimental method has been applied (Wandinger and Ansmann, 2002) to derive the overlap correction vertical profile down to about 400 m. The real part of RI ($RI_{LI}$) has been retrieved from multi-wavelength Raman lidar data, without the use of any a priori assumption. The inversion algorithm is based on the minimum discrepancy criterion and is implemented with the use of regularization techniques (Veselovskii et al., 2002).

Aerosol backscatter coefficient at 355, 532, and 1064 nm and extinction coefficient at 355 and 532 nm have been used in order to obtain the refractive index with an uncertainty of 0.1. The particle extinction coefficient stabilises the solution and decreases the discrepancy of the retrieval. In addition, base functions are used to stabilise the inverted quantity (e.g. the particle refractive index). From the mathematically correct solution space, only the physically meaningful subspace is accepted (Müller et al., 1999). In this study, only solutions with a discrepancy lower than 1% have been considered and the aerosol radius range has been restricted from 0.03 to 10 $\mu$m.

In Figure 6 the $ERI_{COR}$ versus the $RI_{LI}$ for six coinciding OPC-SMPS and lidar measurements is shown. We observe that $ERI_{COR}$ and $RI_{LI}$ are reasonably correlated ($R^2$ = 0.6 for a linear fit). The RH during the lidar measurements in Figure 6 ranged from 40 to 65%, increasing the discrepancy between $ERI_{COR}$ and $RI_{LI}$. We observe that the RH has little effect on the correlation of $ERI_{COR}$ and $RI_{LI}$ for the measurements presented in Figure 6. We may thus conclude that the main mechanism that influences the $ERI_{COR}$ and $RI_{LI}$ correlation is the state of mixing in the vertical. Hygroscopicity data were not availiabe for all measurements shown in Figure 6 and could not be included.

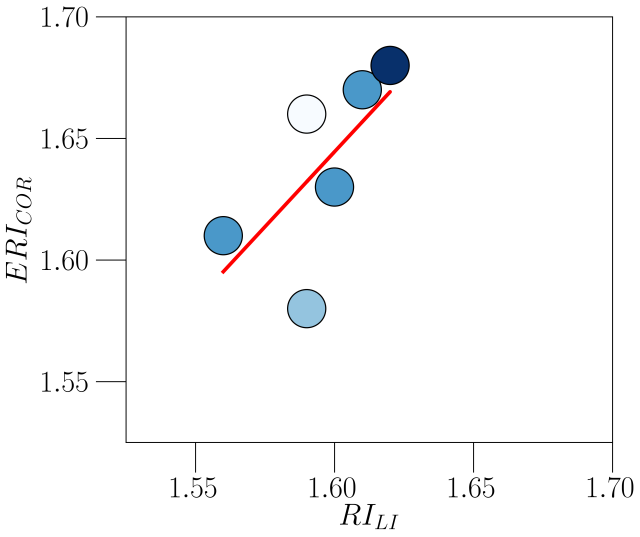


Figure 6: $ERI_{COR}$ to $RI_{LI}$ values. The red line depicts the linear fit for the data points. The color corresponds to RH measured between 1 to 1.2 km a.g.l. (darker blue means higher RH value).

## 6. Summary and Conclusions

As indicated in Figure 3, the $ERI_{COR}$ is influenced strongly by dust light scattering and absorption, in the size range that $ERI_{COR}$ is defined (accumulation mode). During Sahara dust events, $ERI_{COR}$ values approach values as high as 1.7.

As the sulfur per organic carbon ratio increases, $ERI_{COR}$ increases. However, this could not be easily attributed to these two constituents alone, as high values of OC at DEM station usually are associated with high EC values, the main absorbing constituent in aerosols.

$ERI_{COR}$ overestimates RI in relation to $RI_{IC}$. Nevertheless, correlation between the estimated values from the two methods is very good. Higher EC concentration leads to lower $ERI_{COR}$, regardless of dust concentration.

$ERI_{COR}$ relation to $RI_{LI}$ is more complex. $RI_{LI}$ values were obtained at a height between 1 to 1.2 km. There was good mixing in the vertical during chosen days, therefore a good correlation between $ERI_{COR}$ and $RI_{LI}$ is expected (Figures S12-S16). There is also the RH difference problem between the station measurements and those made by the lidar, that increases the discrepancies. Nevertheless, the main difference should be attributed to the state of mixing in the ver-

tical, as indicated in Figure 6.

Overall, the SMPS-OPC system is considered a valuable method so as to estimate real part of RI for ambient aerosol. This is supported by the chemical composition RI ($RI_{IC}$) and $RI_{LI}$ when there is good mixing in the atmosphere. Considering that many stations have long series of SMPS and OPC data, deriving $ERI_{COR}$ could provide valuable information on aerosol properties.

Further work on the subject should include acquiring detailed aerosol composition of PM1, in order to estimate RI corresponding to $ERI_{COR}$. The imaginary part of the $ERI_{COR}$ should be estimated along with the real part, based on SMPS, OPC, EC/OC and AE33 measurements. A model to estimate the imaginary part and the real part of RI could be derived, based on the measurements from the above mentioned instruments.

## Acknowledgements

The authors gratefully acknowledge Professor George Kallos, as the dust mass concentration output of SKIRON model was used to quantify the Sahara dust influence on aerosol measurements in the GAA.

This research has been co-funded by the EnTeC FP7 Capacities program (REGPOT-2012-2013-1, FP7 (ID:316173 )) and partly by People Program (ITN Marie Curie Actions) REA GA no 289923 (ITARS).

Development of lidar retrieval algorithms was supported by Russian Science Foundation; (project No 16-17-10241).

## References

Amato, F., Alastuey, A., Karanasiou, A., Lucarelli, F., Nava S., Calzolai, G., Severi, M., Becagli, S., Gianelle, V. L., Colombi, C., Alves, C., Custódio, D., Nunes, T., Cerqueira M., Pio, C., Eleftheriadis, K., Diapouli, E., Reche, C., Minguillón, M. C., Manousakas, M.-I., Maggos, T., Vratolis S., Harrison, R. M., Querol, X., 2016. AIRUSE-LIFE+: a harmonized PM speciation and source apportionment in five southern European cities. Atmos. Chem. Phys. 16, 3289–3309.

Banks, R. F., Tiana-Alsina, J., Baldasano, J. M., Rocadenbosch F., Papayannis, A., Solomos, S., Tzanis, C. G., 2016. Sensitivity of boundary-layer variables to PBL schemes in the WRF model based on surface meteorological observations, lidar, and radiosondes during the HygrA-CD campaign. Atmos. Res. 176-177(10), 185–201.

Bohren, C., Huffman, D. R., 1998. Absorption and Scattering of Light by Small Particles. Wiley Science Paperback Series.

Bougiatioti, A., Argyrouli, A., Solomos, S., Vratolis, S., Eleftheriadis, K., Papayannis, A., Nenes, A., 2017. CCN Activity, Variability and Influence on Droplet Formation during the HygrA-Cd Campaign in Athens. Atmosphere 8 (108).

Bukowiecki, N., Zieger, P., Weingartner, E., Juranyi, Z., Gysel, M., Neininger, B., SCHNEIDER, B., Hueglin, C., Ulrich, A., Wichser, A., Henne, S., Brunner, D., Kaegi, R., Schwikowski, M., Tobler, L., Wienhold, F. G., Engel, I., Buchmann, B., Peter, T., Baltensperger, U., 2011. Ground-based and airborne in-situ measurements of the Eyjafjallaj okull volcanic aerosol plume in Switzerland in spring 2010. Atmos. Chem. Phys. 11, 10011–10030.

Coen, M., Weingartner, E., Schaub, D., Hueglin, C., Corrigan, C., Henning, S., Schwikowski, M., Baltensperger, U., Dec. 2004. Saharan dust events at the Jungfraujoch: detection by wavelength dependence of the single scattering albedo and first climatology analysis. Atmos. Chem. Phys. 4, 2465–2480.

Emmanouil, C., Drositi, E., Vasilatou, V., Diapouli, E., Krikonis, K., Eleftheriadis, K., Kungolos, A., 2017. Study on particulate matter air pollution, source origin, and human health risk based of $PM_{10}$ metal content in Volos City. Toxicol. Environ. Chem., 1–19.

Flocas, H. A., Helmis, C. G., Blikas, S. N., Asimakopoulos, D. N., Bartzis, J. G., Deligiorgi, D. G., 1998. Mean Characteristics of the Katabatic Flow of a 1024 m High Knife Edge Mountain. Theor. Appl. Climatol. 59, 237–249.

Fountoukis, C., Nenes, A., 2007. ISORROPIAII: A computationally efficient thermodynamic equilibrium model for K+-Ca2+-Mg2+-NH4 +-Na+-SO42–NO3 –Cl–H2O aerosols. Atmos. Chem. Phys. 7 (17), 4639–4659.

Fuller, K. A., Malm, W. C., Kreidenweis, S. M., 1999. Performance evaluation of three optical particle counters with an efficient "multimodal" calibration method. J. Geophys. Res. 104(D13), 15941–15954.

Grimm-Aerosoltechnik, 2005. Portable Dust Monitor SERIES 1.100.

Hand, J. L., Kreidenweis, S. M., 2002. A New Method for Retrieving Particle Refractive Index and Effective Density from Aerosol Size Distribution Data. Aerosol Sci. Technol. 99, 3247–3259.

Hasan, H., Dzubay, T. G., 1983. Apportioning light extinction coefficients chemical species in atmospheric aerosol. Atmos. Environ. 17 (8), 1573–1581.

Heim, M., Mullins, B. J., Umhauer, H., Kasper, G., 2008. Effects of Mixing on Extinction by Carbonaceou s Particles. J. Aerosol Sci 39, 1019–1031.

Hulst van de, H., 1981. Light Scattering by Small Particles. Dover Publications, Inc. New York.

Kallos, G., Papadopoulos, A., Katsafados, P., Nickovic, S., 2006. Transatlantic Saharan dust transport: Model simulation and results. J. Geophys. Res. 111 (D09204).

Kandler, K., Benker, N., Bundke, U., Cuevas, E., Ebert, M., Knippertz, P., Rodrguez, S., Schutz, L., Weinbruch, S., 2007. Chemical composition and complex refractive index of Saharan Mineral Dust at Izan˜a, Tenerife (Spain) derived by electron microscopy. Atmos. Environ. 41, 8058–8074.

Kokkalis, P., Papayannis, A., Mamouri, R., Tsaknakis, G., Amiridis, V., 2012. The EOLE lidar system of the National Technical University of Athens. Proc. 26th International Laser Radar Conference (26th ILRC), Porto Heli, Greece, 629–632.

Lymperopoulos, Y., 2015. Personal communication. Grimm Aerosoltechnik.

Mamouri, R., Papayannis, A., Tsaknakis, G., Amiridis, V., 2007. Six-month ground-based water vapour Raman lidar measurements over Athens, Greece and system validation. J. Optoel. Adv. Materials 9, 3546–3549.

Mamun, M. M., Müller, D., 2016. Retrieval of Intensive Aerosol Microphysical Parameters from Multiwavelength Raman/HSRL Lidar: Feasibility Study with Artificial Neural Networks. Atmos. Meas. Tech. Discuss. 7.

Mantas, E., Remoundaki, E., Halari, I., Kassomenos, P., Theodosi, C., Hatzikioseyian, A., Mihalopoulos, N., 2014. Mass closure and source apportionment of $PM_{2.5}$ by Positive Matrix Factorization analysis in urban Mediterranean environment. Atmos. Environ. 94, 154–163.

Mätzler, C., june 2002. MATLAB Functions for Mie Scattering and Absorption. Institude of Applied Physics, University of Bern, Research Report 2002-08.

Müller, D., Wandinger, U., Ansmann, A., 1999. Microphysical particle parameters from extinction and backscatter lidar data by inversion with regularization: theory. Appl. Opt. 38(12), 2346–2357.

Nava, S., Becagli, S., Calzolai, G., Chiari, M., Lucarelli, F., Prati, P., Traversi, R., Udisti, R., Valli, G., Vecchi, R., 2012. Saharan dust impact in central Italy: An overview on three years elemental data records. Atmos. Environ. 60, 444–452.

Nelder, J. A., Mead, R., 1965. A simplex method for function minimization. COMPUT J 7, 308–313.

Panteliadis, P., Hafkenscheid, T., Cary, B., Diapouli, E., Fischer, A., Favez, O., Quincey, P., Viana, M., Hitzenberger, R., Vecchi, R., Saraga, D., Sciare, J., Jaffrezo, J. L., John, A., Schwarz, J., Giannoni, M., Novak, J., Karanasiou, A., Fermo, P., Maenhaut, W., 2015. ECOC comparison exercise with identical thermal protocols after temperature offsets correction – instrument diagnostics by in-depth evaluation of operational parameters. Atmos. Meas. Tech. 8(2), 779–792.

Papayannis, A. D., Argyrouli, A., Bougiatioti, A., Remoundaki, E., Vratolis, S., Nenes, A., Solomos, S., Komppula, M., Giannakaki, E., Kalogiros, J. A., Banks, R. F., Eleftheriadis, K., Mantas, E., Diapouli, E., Tzanis, C. G., Kazadzis, S. A., Binietoglou, I., Labzovski, L. N., Vande Hey, J. D., Zerefos, C. S., 2017. An overview from hygroscopic aerosols to cloud droplets: The HygrA-CD campaign in the Athens basin . Sci. Total Environ. 574, 216–233.

Schneider, F., 2016. Personal communication.

Stelson, A. W., 1990. Urban Aerosol Refractive Index Prediction by Partial Molar Refraction Approach. Environ. Sci. Technol. 24, 1676–1679.

Sultanova, N., Kasarova, S., Nikolov, I., 2009. Dispersion Properties of Optical Polymers. Acta Phys. Pol. A 116.

Tang, I., 1996. Chemical and size effects of hygroscopic aerosols on light scattering coefficients. J. Geophys. Res. 101, 19245 – 19250.

TOPAS, 2008. Di-Ethyl_Hexyl_Sebacat. Excerpt from the Producer's Material Safety Data Sheet (29 June 2008).

Veselovskii, I., Kolgotin, A., Griaznov, V., Muller, D., Wandinger, U., Whiteman, D. N., 2002. Inversion with regularization for the retrieval of tropospheric aerosol parameters from multiwavelength lidar sounding. Appl. Opt. 41(18), 3685–3699.

Wandinger, U., Ansmann, A., Jan. 2002. Experimental determination of the lidar overlap profile with Raman lidar. Appl Opt 41 (3), 511–4.

Wiedensohler, A., Birmili, W., Nowak, A., Sonntag, A., Weinhold, K., Merkel, M., Tuch, B. W. T., Pfeifer, S., Fiebig, M., Fjäraa, A. M., Asmi, E., Sellegri, K., Depuy, R., Venzac, H., Villani, P., Laj, P., Aalto, P., Ogren, J. A., Swietlicki, E., Williams, P., Roldin, P., Quincey, P., Hüglin, C., Fierz-Schmidhauser, R., Gysel, M., Weingartner, E., Riccobono, F., Santos, S., Grüning, C., Faloon, K., Beddows, D., Harrison, R., Monahan, C., Jennings, S. G., O'Dowd, C. D., Marinoni, A., Horn, H.-G., Keck, L., Jiang, J., Scheckman, J., McMurry, P. H., Deng, Z., Zhao, C. S., Moerman, M., Henzing, B., de Leeuw, G., Löschau, G., Bastian, S., 2012. Mobility particle size spectrometers: harmonization of technical standards and data structure to facilitate high quality long-term observations of atmospheric particle number size distributions. Atmos. Meas. Tech. 5, 657–685.